Supporting Information

Multifunctional Transparent Conductive Films by Langmuir-Blodgett Assembly of Large MXene Flakes

Jie Xue,†[a] Dan liu,†[a] Chuanbing Li,[a] Zifu Zhu,[a] Yuxuan Sun,[a] Xiaobo Gao,[a] and Qingbin Zheng*[a]

[a]School of Science and Engineering, The Chinese University of Hong Kong, Shenzhen, Guangdong 518172, China.

*Correspondence and requests for materials should be addressed to Qingbin Zheng (zhengqingbin@cuhk.edu.cn)

Experimental Section

Size Screening of Ti_3AlC_2 MAX Phase: Large Ti_3AlC_2 MAX phase was firstly obtained based on gravity sedimentation.[1] 5 g as-received Ti_3AlC_2 MAX phase powder (200 mesh, 11 Technology Co., Ltd) was stirred continuously in 200 mL deionized water with a height of 8 cm for 10 min. After allowing it to remain undisturbed for 400 s, the upper dispersion containing small MAX particles were removed. The stirring and standing process was repeated three times, and the sediment with MAX particles larger than 10 μm were collected and subsequently dried in an electrothermal blowing oven for further use. The standing time was determined by the settling velocity (v, m s^{-1}), which can be expressed as follows.

$$v = \frac{2(\rho_p - \rho_f)gR^2}{9\mu} \#\ (S1)$$

where ρ_p and ρ_f are the mass density of MAX phase particles (4.2×10^3 kg m^{-3}) and water (1.0×10^3 kg m^{-3}), respectively, μ is the dynamic viscosity of water (8.9×10^{-4} Pa s under 25 °C), g indicates the gravitational acceleration (9.8 m s^{-2}), and R denotes the radius of spherical particles (m).

Synthesis of $Ti_3C_2T_x$ MXene Flakes: Firstly, 1.6 g lithium fluoride (LiF 99%, Macklin) was completely dissolved in 20 mL 9 M hydrochloric acid (HCl) in a Teflon container with continuous stirring. Then, 1.0 g pre-screened Ti_3AlC_2 MAX powder was slowly added into the LiF/HCl etching solution, which were stirred continuously for 36 h at 50 °C. The obtained suspension was subjected to repeated washing with HCl (1 M), followed by deionized water, until the pH value of the supernatant approached ~6.0. After that, self-delamination of multilayer $Ti_3C_2T_x$ occurred. Subsequently, 40 mL deionized water was poured into the muddy sediment, followed by manual shaking to re-disperse and centrifuging to precipitate without decanting the upper suspension. The

process of gentle shaking and centrifugation was repeated five times to increase the yield of $Ti_3C_2T_x$ flakes. The obtained dispersion was centrifuged under 1500 rpm for 30 min to collect the spontaneously delaminated $Ti_3C_2T_x$ flakes. Finally, the upper dark green suspension was further centrifuged under 4500 rpm for 20 min to collect the sediment, labeled as large $Ti_3C_2T_x$ MXene (LM) flakes. To obtain small $Ti_3C_2T_x$ MXene (SM) flakes, the neutral dispersion after washing was subjected to a probe sonication in an ice bath lasting for 40 min (30% amplitude, 2 s on/4 s off), followed by centrifugation at 1500 rpm for 30 min to collect the supernatant solution.

Preparation of M-TCFs based on SLMFs by LB Assembly: In a typical experiment, a KSV NIMA Langmuir-Blodgett trough (KN 2002) with an area of 273 cm^2 was firstly carefully cleaned with ethanol. Then, 0.01 M HCl (pH = 2.0) was added as the subphase. To spread $Ti_3C_2T_x$ flakes on the subphase surface, methanol, a polar alcohol, was mixed with water in an optimal ratio of 5:1 to prepare 0.1 mg mL^{-1} $Ti_3C_2T_x$ dispersion. The $Ti_3C_2T_x$ dispersion was dropwise spread on the water under a rate of 100 μL min^{-1} using a glass syringe, reaching a total volume of 5 mL. After stabilization for 10 min, the $Ti_3C_2T_x$ flakes floated on the water were compressed with two barriers moving at a pace of 10 mm min^{-1}, while the real-time surface pressure was monitored by a Wilhelmy plate suspended from a feedback-equipped tensiometer. When the preset surface pressure was reached, the assembled films were vertically transferred onto targeted substrates, including glass or polymer. Before deposition, the substrate was cleaned with the Piranha solution comprising of sulfuric acid (H_2SO_4) and peroxide (H_2O_2) with a volume ratio of 7:3 for 30 min to obtain a hydrophilic surface for proper wetting and efficient transfer. The hydrophilic substrate was pre-impregnated in the subphase and then pulled out under a rate of 0.1 mm min^{-1} when the preset value of surface pressure was reached. As the meniscus spread over the surface of substrates, SLMFs were transferred onto the substrate from the air-water interface, which could be utilized as

M-TCFs. Multilayer films were prepared by multiple transfer steps onto the substrate under the same conditions. Each layer was dried under vacuum overnight or baked under 60 °C in vacuum for 1 h to guarantee the adhesion of the SLMF with the substrate.

Morphological and Structural Characterizations: SEM (TESCAN MAIA3), TEM (JEOL JEM-F200) and OM (Olympus BX53M) were used to characterize the morphology of assembled SLMFs at various stages. The SAED pattern and lattice fringes of $Ti_3C_2T_x$ flake were detected by HR-TEM (FEI Tecnai G2 Spirit 120kV). AFM (Bruker MultiMode 8) was utilized to evaluate the surface morphology of SLMFs and their thickness at low surface pressure. The thickness of multilayer films was obtained by FIB-SEM (TESCAN SOLARIS GMH). XRD (Rigaku SmartLab) was employed to detect the change of crystal structure in the preparation process of $Ti_3C_2T_x$ flakes and under different annealing temperatures. XPS (Shimadzu AXIS SUPRA+) was used to analyze the elemental components at different annealing temperatures. An optical contact angel meter (Dataphysics OCA25) was utilized to evaluate the wettability of the films.

Optoelectrical Property Measurements: The transmittance of SLMFs on glass substrates were measured on an ultraviolet-visible spectrophotometer (Shimadzu UV3600Plus) covering the wavelength range of 200–1000 nm. The sheet resistance of LB assembled SLMFs was determined on a digital four-point probe tester (Suzhou Jingge ST2253) and the distance between adjacent probes is 2 mm. The four points at which the probe contacts the film were coated with conductive silver paste to mitigate contact resistance.

Joule Heating Measurements: Two silver wires were connected at either end of the sample (2.0 × 1.0 cm^2) with the aid of conductive silver paste for clamping to apply voltage provided by a DC Source (Nanjing Maynuo M8813). The real-time surface temperature and thermal images were

captured using an infrared camera (FLIR E95). The distance between the IR camera and the film was approximately 10 cm.

Electromagnetic Interference Shielding Measurements: The SLMFs were transfer onto glass wafers (22.86 mm × 10.16 mm × 0.5 mm) for EMI shielding tests conducted on a vector network analyzer (Keysight P5004A) over a frequency range of 8.2–12.4 GHz (X-band). Scattering parameters (S_{11}, S_{22}, S_{12}, and S_{21}) can be directly obtained during testing, from which reflection (R), transmission (T) and absorption (A) occurred in the propagation of EM waves can be derived as follows.

$$R = |S_{11}|^2 \#（S2）$$

$$T = |S_{12}|^2 \#（S3）$$

$$A = 1 - R - T \#(S4)$$

The SE_R, SE_A and SE_T can be calculated from the measured R and T coefficients, as presented in Equation S5-S7.

$$SE_R = -10\log(1 - R) \#(S5)$$

$$SE_A = -10\log\left(\frac{T}{1 - R}\right) \#(S6)$$

$$SE_T = -10\log T \#(S7)$$

To evaluate the SSE/t, the mass of assembled films transferred onto the substrate ($Mass_{film}$) should be firstly calculated. Since $Ti_3C_2T_x$ flakes are uniformly spread on the water, $Mass_{film}$ can be determined as follows.

$$Mass_{film} = 0.5\ mg \times \frac{Area_{glass}}{Area_{trough}} \#(S8)$$

where 0.5 mg is the total quantity of $Ti_3C_2T_x$ added, $Area_{glass}$ represents the area of the transferred glass substrate, which is fixed at 22.86 × 10.16 mm^2. $Area_{trough}$ is the area of the trough at a given surface pressure derived from the surface pressure-area isothermal curve, corresponding to the extent of SLMF coverage over the water surface.

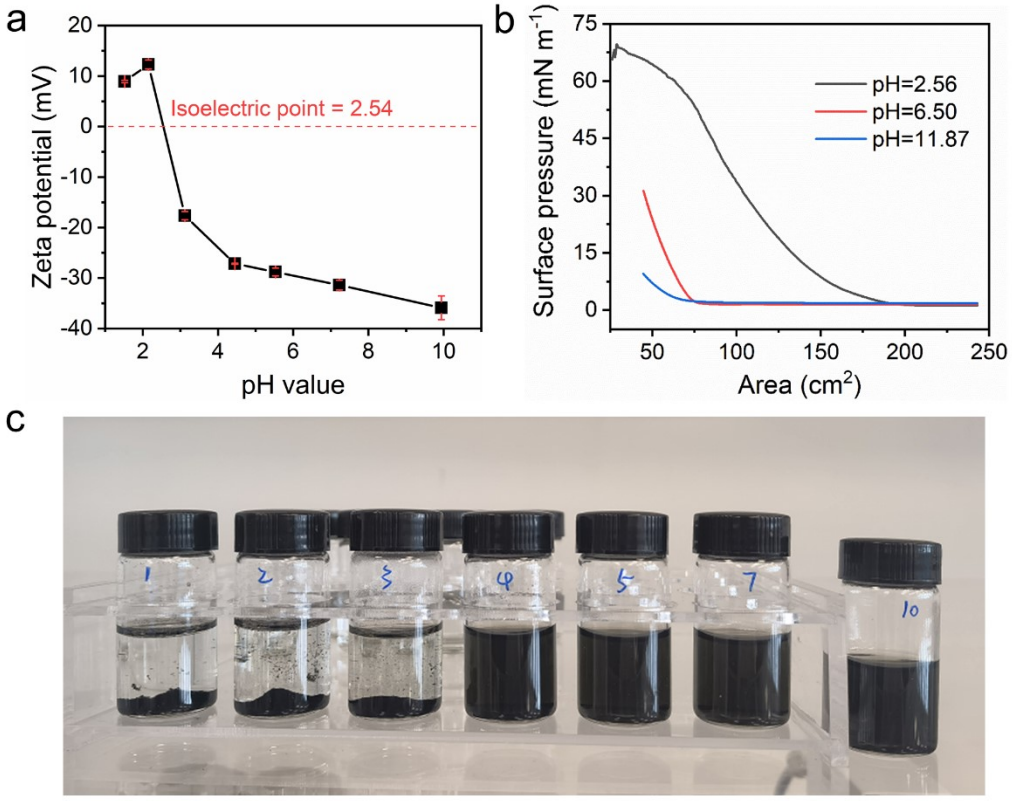

Figure S1 (a) Zeta potential of LM flakes measured in 0.02 mg ml^{-1} aqueous dispersions. The isoelectric point (the pH value at zero potential) was 2.54. (b) Surface pressure-area isotherm curves of LM flakes recorded at subphase with different pH values. (c) LM aqueous dispersions with different pH values (from 1.52 to 9.94, labeled as from 1 to 10) after standing for 1 day. The flakes dispersed in a pH value near the isoelectric point (from 1.52 to 3.12, labeled as from 1 to 3) displayed notable precipitation within 5 min.

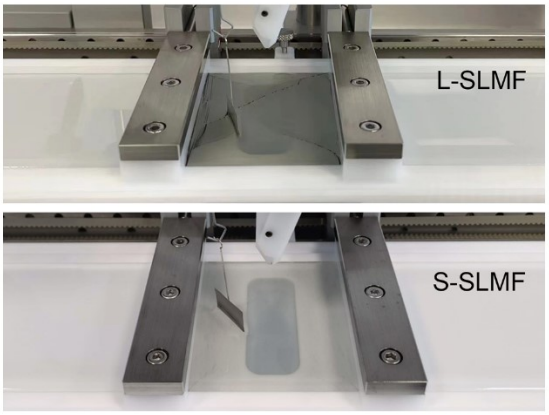

Figure S2 Comparison of LB assembled SLMFs with LM flakes (top) and SM flakes (bottom) when the surface area was compressed to less than 50 cm^2.

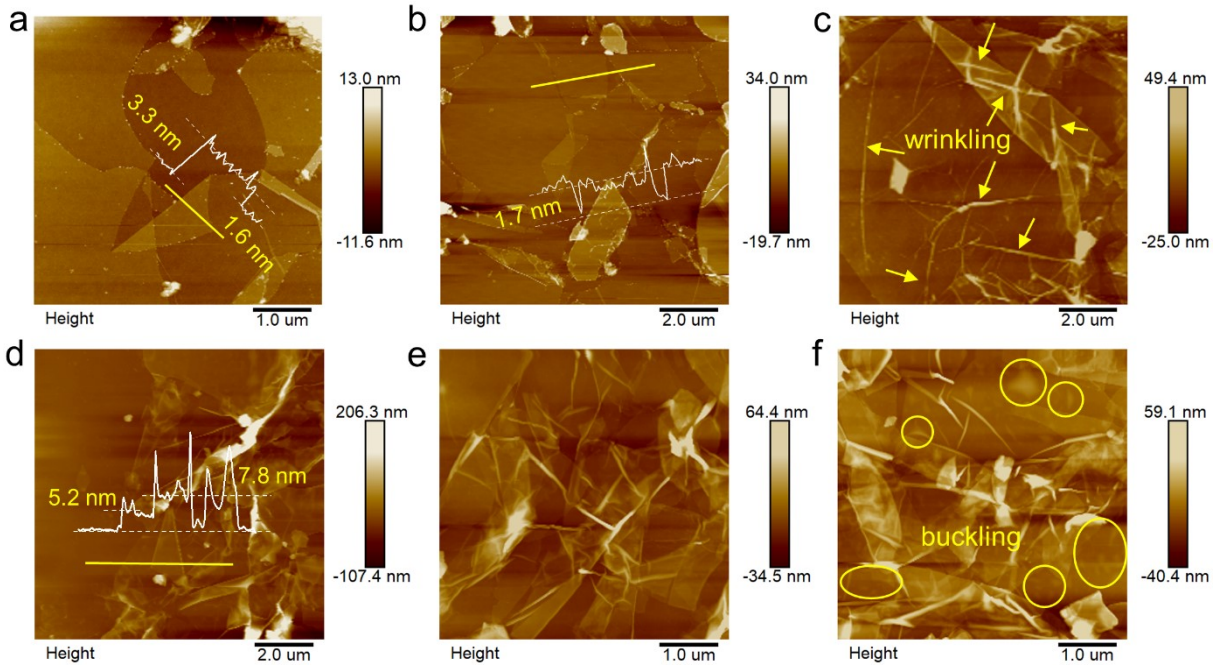

Figure S3 AFM images of (a) the margin and (b) the surface of L-SLMF-2 at a pulling speed of 0.1 mm min^{-1}, as well as (c) the surface of of L-SLMF-2 at a pulling speed of 1.0 mm min^{-1}. AFM images of (a) the margin and (b) the surface of L-SLMF-4 at a pulling speed of 0.1 mm min^{-1}, as well as (c) the surface of of L-SLMF-4 at a pulling speed of 1.0 mm min^{-1}.

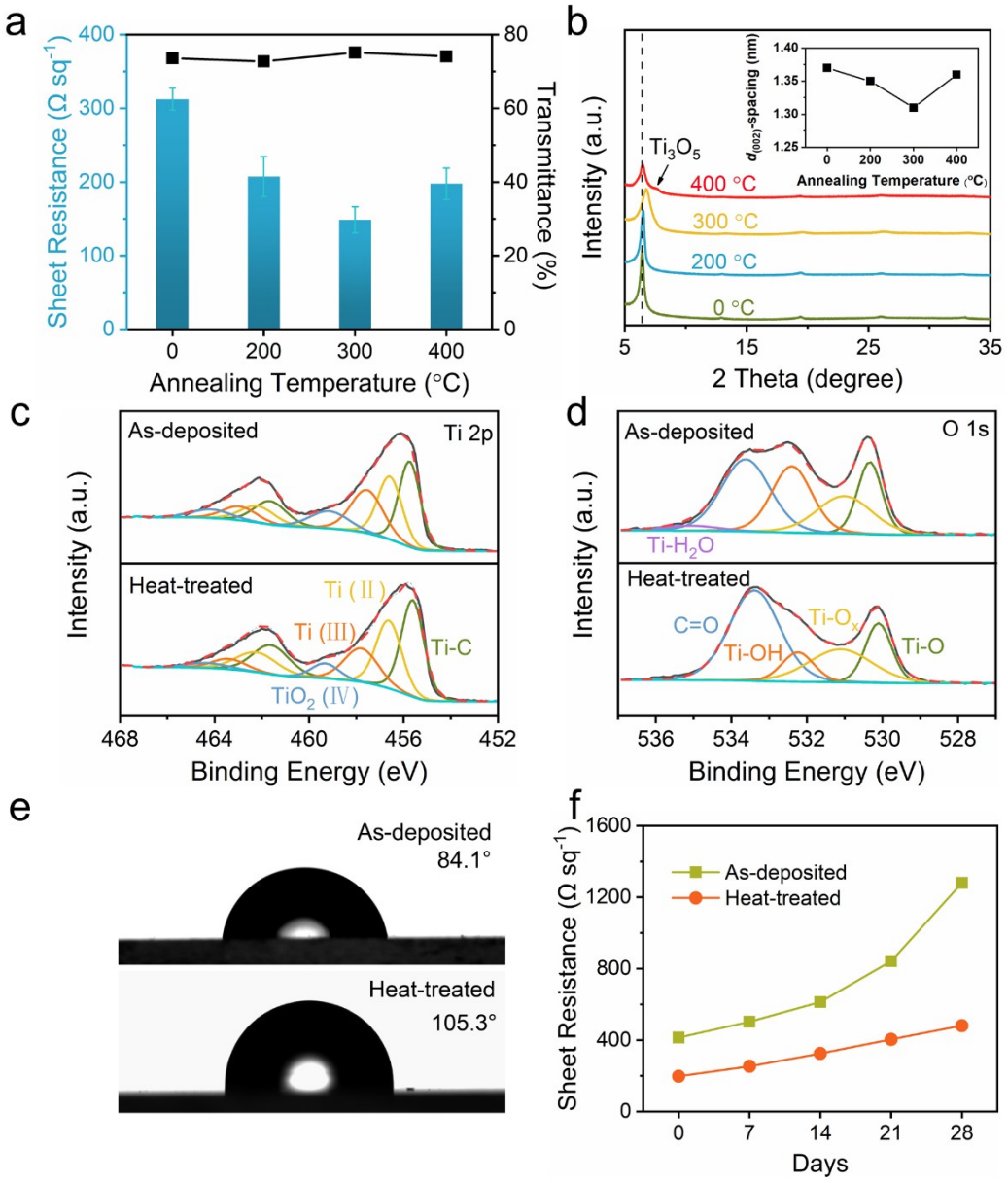

Figure S4 (a) The changes of sheet resistance and optical transmittance at 550 nm of L-SLMF-4 under various annealing temperatures. (b) XRD patterns and $d_{(002)}$-spacing evolutions of L-SLMF-4 under various annealing temperatures. (c) Ti 2p and (d) O 1s XPS spectra of L-SLMF-4 before and after 300 ℃ thermal treatment. (e) Water contact angle measuremets and (f) sheet resistance changes under ambient conditions of L-SLMF-4 before and after 300 ℃ thermal treatment.

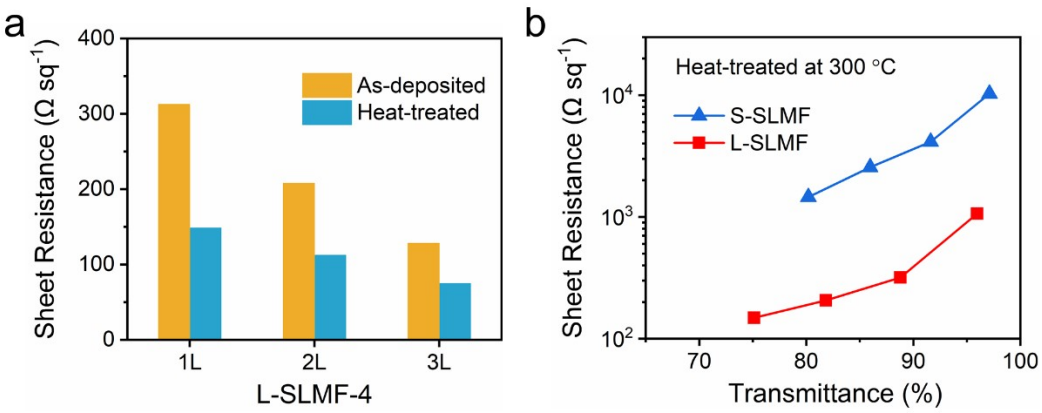

Figure S5 (a) Sheet resistance changes of L-SLMF-4 with various numbers of layers before and after 300 °C thermal treatment. (b) Sheet resistance and optical transmittance at 550 nm for various SLMFs after 300 °C thermal treatment.

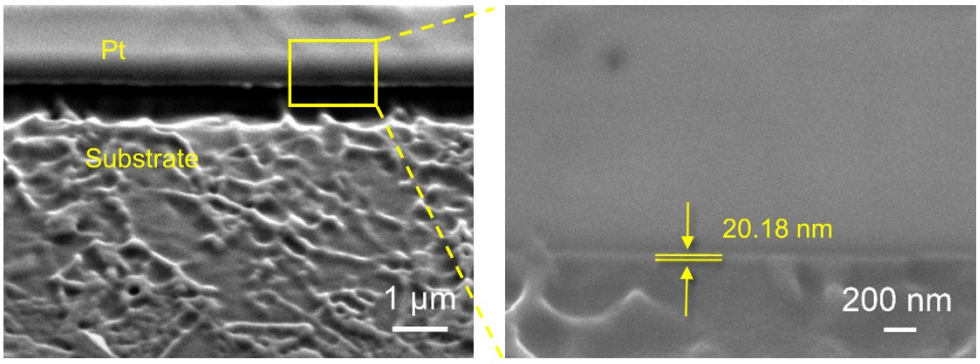

Figure S6 Cross-sectional FIB-SEM images of L-SLMF-4 with three layers.

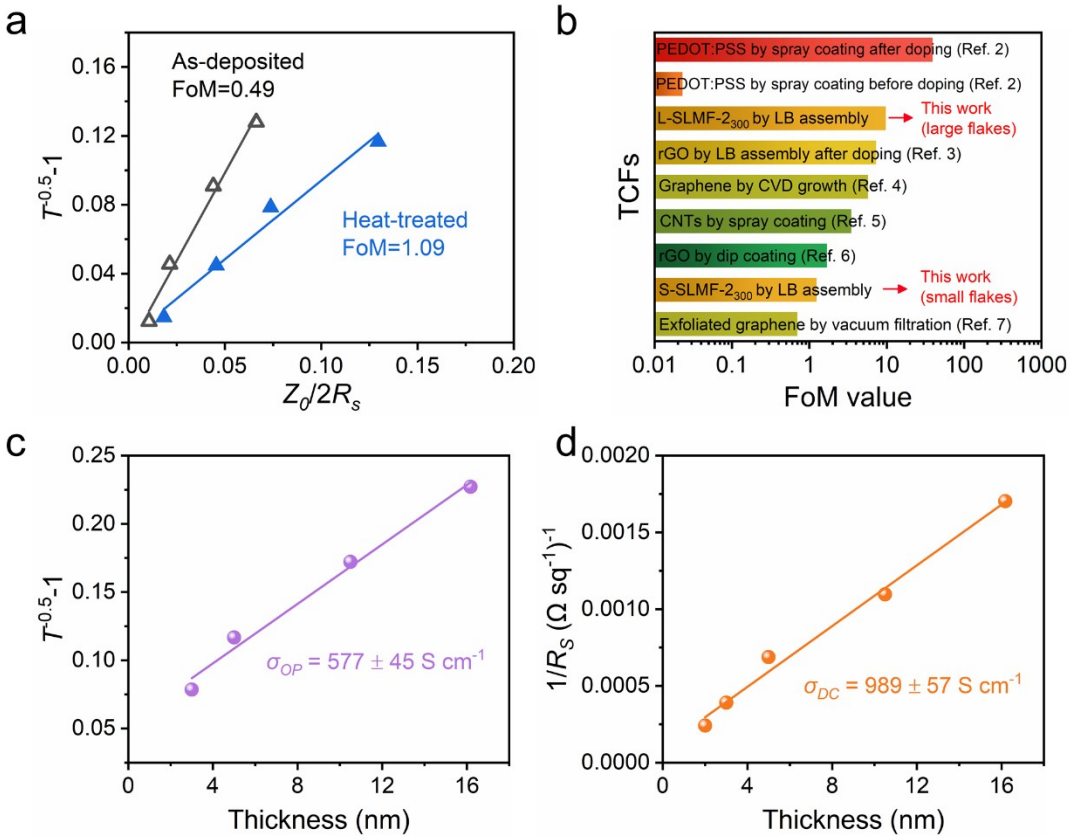

Figure S7 Optoelectrical properties of S-SLMFs. (a) Plot of $T^{-1/2} - 1$ vs. $Z_o/2R_S$, and the slope of the fitted curve is equal to FoM^{-1}. (b) Comparison of FoM of various TCFs, including PEDOT:PSS by spray coating after and before doping,[2] rGO by LB assembly after doping,[3] graphene by CVD growth,[4] CNTs by spray coating,[5] rGO by dip coating,[6] and exfoliated graphene by vacuum filtration.[7] (c) Plot of $T^{-1/2} - 1$ vs. t and (d) Plot of $1/R_s$ vs. t to give σ_{OP} and σ_{DC}, respectively.

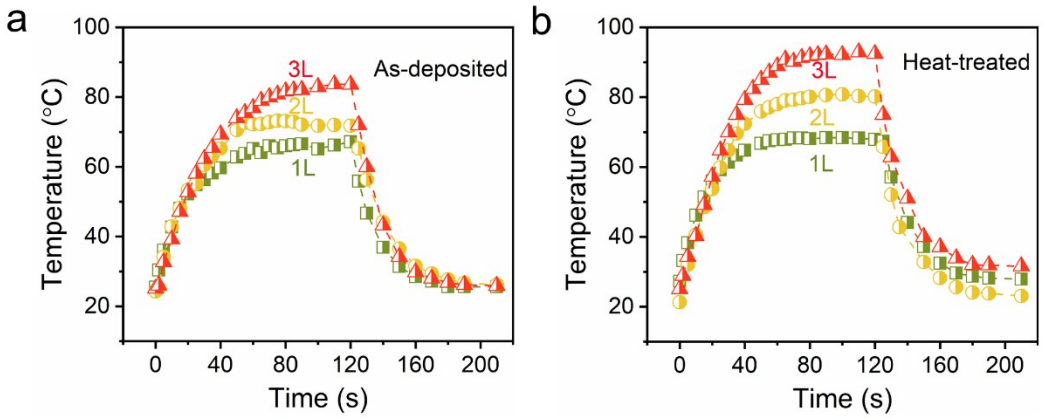

Figure S8 Electrical heating performance of L-SLMF-4 with various numbers of layers (a) before and (b) after 300 °C thermal treatment at an applied DC voltage of 15 V.

Figure S9 EMI SE_T values in X-band range of L-SLMF-4 with various numbers of layers (a) before and (b) after 300 °C thermal treatment.

Table S1 Calculation of the area coverage fraction of SLMFs.

Sample	Pixel of Substrate	Film coverage fraction (%)
L-SLMF-1	794314	67.31
L-SLMF-2	81853	96.63
L-SLMF-3	31819	98.69
L-SLMF-4	0	100
S-SLMF-1	953774	60.75
S-SLMF-2	451819	81.40
S-SLMF-3	211959	91.28
S-SLMF-4	399	99.98

Total pixel of each image: 1800 × 1350

Table S2 Comparison of the optoelectrical properties of single-layer $Ti_3C_2T_x$ MXene films prepared by self-assembly.

Size	Fabrication method	Transmittance at 500 nm (%)	Sheet resistance (Ω sq-1)	σ_{DC}/σ_{OP}	Application	Reference
＜5 μm	Lateral self-assembly	91.2 (1L) 84.14 (2L) 82.22 (3L)	10000 5000 4000	0.3999 0.418 0.458	/	8
＜5 μm	Lateral self-assembly	78 (1L) 50 (3L)	650 150	2.198 3.034	Gas sensing	9
1 μm	Layer-by-layer assembly	65	900	0.87	Supercapacitors	10
~500 nm	Langmuir-Blodgett assembly	90 (1L) 60 (10L)	40000 350	0.087 1.851	Supercapacitors	11
0.25 μm^2	Langmuir-Blodgett assembly	97 92 86 80	10280 4139 2557 1455	1.09 (fitting)	/	This work (small flakes)
52.01 μm^2	Langmuir-Blodgett assembly	96 89 82 75	1064 318 206 148	8.16 (fitting)	Joule heating and EMI shielding	This work (large flakes)

Table S3 Specific EMI SE normalized by thickness of various shielding materials.

Type	Filler	Matrix	Thickness (cm)	SE (dB)	SSE (dB cm^3 g^{-1})	SSE/t (dB cm^2 g^{-1})	Reference
CNTs	A-CNT	PANI	0.0005	50.2	37.5	7.94×10^4	12
	CNT	Nanofibers	0.0048	24.6	60	1.25×10^4	13
	SWCNT	MWCNT	0.013	65	79.3	6.10×10^4	14
	CNT sponge	PDMS	0.18	54.8	5480	3.04×10^4	15
	CNT aerogel film		0.0024	51	-	2.0×10^5	16
Metals	Ag nanowire	Carbon	0.3	70.1	18350.8	6.12×10^4	17
	Ag nanowire aerogel		0.05	109.3	-	3.53×10^5	18
	Ag nanofiber		0.0001	20	1000	1.00×10^6	19
			0.01	76	380	3.80×10^4	
	Al Foil		0.0008	66	24.4	3.06×10^4	20
	Cu Foil		0.001	70	7.8	7.81×10^3	20
	CuNi		0.15	25	104	690	21
Graphenes	rGO/Fe_3O_4		0.03	24	31	1.03×10^3	22
	Graphene	PEN	0.0003	20	21.89	7.30×10^4	23
	rGO/Co/C	Carbon fiber	0.01	38.46	143.8	1.44×10^4	24
	PEDOT:PSS	rGO	0.15	91.9	1206	8.04×10^3	25
	Graphene	PDMS	0.1	20	500	5.00×10^3	26
	Graphene/CNTs		0.16	36	370.8	2.32×10^3	27
	Graphene/CNTs		0.16	38	6600	4.00×10^4	28
	GO aerogel		0.32	35.9	-	6.72×10^4	29
	$Ti_3C_2T_x$/rGO film		0.006	59	-	3.76×10^4	30
	Graphene aerogel film		0.006	90	219.5	1.83×10^4	31
MXenes	$Ti_3C_2T_x$	Cellulose	0.0074	25.8	19.5	2.65×10^3	32
	$Ti_3C_2T_x$ aerogel	PDMS	0.01	45.8	-	1.78×10^4	33
	$Ti_3C_2T_x$		0.00025	50	20.9	8.37×10^4	20
			0.0011	68	28.4	2.59×10^4	
			0.0045	92	38.5	8.56×10^3	
	$Ti_3C_2T_x$		0.1	44.8	8145.5	8.15×10^4	34
	Ti_2CT_x			48.5	8818.2	8.82×10^4	
	Ti_3CNT_x			42.3	7690.9	7.69×10^4	
	$Ti_3C_2T_x$ foam		0.0006	32	82	1.37×10^5	35
			0.0018	50	125	6.94×10^4	
			0.006	70	318	5.30×10^4	
	$Ti_3C_2T_x$ film		0.001	54.42	-	3.54×10^4	36
			0.001	50.11		3.05×10^4	
			0.001	39.77		2.64×10^4	
	$Ti_3C_2T_x$ film		2.1×10^{-7}	3.37	0.17	7.86×10^5	This work
			4.0×10^{-7}	4.06	0.28	7.11×10^5	
			6.58×10^{-7}	4.37	0.31	4.75×10^5	
			1.25×10^{-6}	9.02	0.61	4.90×10^5	
			2.02×10^{-6}	11.45	0.84	4.14×10^5	

References

1. J. Zhang, N. Kong, S. Uzun, A. Levitt, S. Seyedin, P. A. Lynch, S. Qin, M. Han, W. Yang, J. Liu, X. Wang, Y. Gogotsi and J. M. Razal, *Adv. Mater.*, 2020, **32**, 2001093.
2. T. M. Higgins and J. N. Coleman, *ACS Appl. Mater. Interfaces*, 2015, **7**, 16495-16506.
3. Q. Zheng, W. H. Ip, X. Lin, N. Yousefi, K. K. Yeung, Z. Li and J.-K. Kim, *ACS Nano*, 2011, **5**, 6039-6051.
4. K. S. Kim, Y. Zhao, H. Jang, S. Y. Lee, J. M. Kim, K. S. Kim, J.-H. Ahn, P. Kim, J.-Y. Choi and B. H. Hong, *Nature*, 2009, **457**, 706-710.
5. M. Kaempgen, G. S. Duesberg and S. Roth, *Appl. Surf. Sci.*, 2005, **252**, 425-429.
6. J. Zhao, S. Pei, W. Ren, L. Gao and H.-M. Cheng, *ACS Nano*, 2010, **4**, 5245-5252.
7. A. A. Green and M. C. Hersam, *Nano Lett.*, 2009, **9**, 4031-4036.
8. M. Mojtabavi, A. VahidMohammadi, K. Ganeshan, D. Hejazi, S. Shahbazmohamadi, S. Kar, A. C. T. van Duin and M. Wanunu, *ACS Nano*, 2021, **15**, 625-636.
9. S. J. Kim, J. Choi, K. Maleski, K. Hantanasirisakul, H. T. Jung, Y. Gogotsi and C. W. Ahn, *ACS Appl. Mater. Interfaces*, 2019, **11**, 32320-32327.
10. I. J. Echols, J. Yun, H. Cao, R. M. Thakur, A. Sarmah, Z. Tan, R. Littleton, M. Radovic, M. J. Green and J. L. Lutkenhaus, *Chem. Mater.*, 2022, **34**, 4884-4895.
11. L. Fan, P. Wen, X. Zhao, J. Zou and F. Kim, *ACS Appl. Nano Mater.*, 2022, **5**, 4170-4179.
12. H. Li, X. Lu, D. Yuan, J. Sun, F. Erden, F. Wang and C. He, *J. Mater. Chem. C*, 2017, **5**, 8694-8698.

13. S. X. Song, L. H. Li, D. X. Ji, J. F. Zhao, Q. Wu and Q. Y. Wang, *ACS Appl. Mater. Interfaces*, 2023, **15**, 35495-35506.

14. S. Lu, J. Shao, K. Ma, D. Chen, X. Wang, L. Zhang, Q. Meng and J. Ma, *Carbon*, 2018, **136**, 387-394.

15. D. Lu, Z. Mo, B. Liang, L. Yang, Z. He, H. Zhu, Z. Tang and X. Gui, *Carbon*, 2018, **133**, 457-463.

16. C. Fu, Z. Sheng and X. Zhang, *ACS Nano*, 2022, **16**, 9378-9388.

17. Y. J. Wan, P. L. Zhu, S. H. Yu, R. Sun, C. P. Wong and W. H. Liao, *Small*, 2018, **14**, 1800534.

18. F. Peng, W. Zhu, Y. Fang, B. Fu, H. Chen, H. Ji, X. Ma, C. Hang and M. Li, *ACS Appl. Mater. Interfaces*, 2023, **15**, 4284-4293.

19. S. Lin, H. Wang, F. Wu, Q. Wang, X. Bai, D. Zu, J. Song, D. Wang, Z. Liu and Z. Li, *npj Flexible Electron.*, 2019, **3**, 6.

20. F. Shahzad, M. Alhabeb, C. B. Hatter, B. Anasori, S. Man Hong, C. M. Koo and Y. Gogotsi, *Science*, 2016, **353**, 1137-1140.

21. K. Ji, H. Zhao, J. Zhang, J. Chen and Z. Dai, *Appl. Surf. Sci.*, 2014, **311**, 351-356.

22. W.-L. Song, X.-T. Guan, L.-Z. Fan, W.-Q. Cao, C.-Y. Wang, Q.-L. Zhao and M.-S. Cao, *J. Mater. Chem. A*, 2015, **3**, 2097-2107.

23. S. Zhang, H. Y. Sun, T. G. Lan, Z. X. Bai and X. B. Liu, *Composites, Part A*, 2022, **154**, 106777.

24. Z. Liu, C. Liu, Y. Wang, M. Song, J. Guo, W. Wang and X. Gao, *Carbon*, 2024, **217**, 118655.

25. N. Yousefi, X. Sun, X. Lin, X. Shen, J. Jia, B. Zhang, B. Tang, M. Chan and J. K. Kim, *Adv. Mater.*, 2014, **26**, 5480-5487.

26. Z. Chen, C. Xu, C. Ma, W. Ren and H. M. Cheng, *Adv. Mater.*, 2013, **25**, 1296-1300.

27. Q. Song, F. Ye, X. Yin, W. Li, H. Li, Y. Liu, K. Li, K. Xie, X. Li and Q. Fu, *Adv. Mater.*, 2017, **29**, 1701583.

28. L. Kong, X. Yin, M. Han, X. Yuan, Z. Hou, F. Ye, L. Zhang, L. Cheng, Z. Xu and J. Huang, *Carbon*, 2017, **111**, 94-102.

29. A. A. Isari, A. Ghaffarkhah, S. A. Hashemi, H. Yousefian, O. J. Rojas and M. Arjmand, *Adv. Funct. Mater.*, 2024, DOI: 10.1002/adfm.202402365, 2402365.

30. Y. Zhang, K. Ruan, X. Shi, H. Qiu, Y. Pan, Y. Yan and J. Gu, *Carbon*, 2021, **175**, 271-280.

31. J. Xi, Y. Li, E. Zhou, Y. Liu, W. Gao, Y. Guo, J. Ying, Z. Chen, G. Chen and C. Gao, *Carbon*, 2018, **135**, 44-51.

32. W.-T. Cao, F.-F. Chen, Y.-J. Zhu, Y.-G. Zhang, Y.-Y. Jiang, M.-G. Ma and F. Chen, *ACS Nano*, 2018, **12**, 4583-4593.

33. S. Kumar Deb, P. Dutta, G. Masud Karim, A. Patra, P. Bera, S. Das, P. Mukherjee, K. Rengasamy, A. Borbora, U. Manna, V. Subramanian and U. Narayan Maiti, *Chem. Eng. J.*, 2024, **484**, 149617.

34. M. Han, X. Yin, K. Hantanasirisakul, X. Li, A. Iqbal, C. B. Hatter, B. Anasori, C. M. Koo, T. Torita and Y. Soda, *Adv. Opt. Mater.*, 2019, **7**, 1900267.

35. J. Liu, H. B. Zhang, R. Sun, Y. Liu, Z. Liu, A. Zhou and Z. Z. Yu, *Adv. Mater.*, 2017, **29**, 1702367.

36. Q. Zhang, R. Fan, W. Cheng, P. Ji, J. Sheng, Q. Liao, H. Lai, X. Fu, C. Zhang and H. Li, *Adv. Sci.*, 2022, **9**, 2202748.